Flexible and Ultra-Thin Glass Substrates for RF Applications

Sridhar Sivapurapu[1], Rui Chen[2], Mutee ur Rehman[1], Kimiyuki Kanno[3], Takenori Kakutani[4], Martin Letz[5], Fuhan Liu[1], Suresh K. Sitaraman[2], and Madhavan Swaminathan[1]
[1]3D Systems Packaging Research Center*, Georgia Institute of Technology, Atlanta, GA USA
*School of Electrical & Computer Engineering, School of Materials Science & Engineering
[2]G. W. Woodruff School of Mechanical Engineering, Georgia Institute of Technology, Atlanta, GA USA
[3]JSR Corporation, 100 Kawajiri-cho, Yokkaichi, Mie 510-8552, Japan
[4]Taiyo Ink Mfg. Co. Ltd., 900 Hirasawa Ranzan-machi, Saitama 355-0215, Japan
[5]SCHOTT AG, Hattenbergstr. 10, 55122 Mainz, Germany

***Abstract*—Glass has been shown to be a capable core substrate material for high frequency applications. In this paper we examine the capabilities of ultra-thin glass as a flexible material that can be used for high frequency flexible applications. The two stack-ups discussed in this paper are 60 µm in total thickness with a core glass substrate (Schott AF32) of 30 µm thickness. One stack-up uses 15 µm JSR GT-N01 as a buildup dielectric and the other uses 15 µm Taiyo Photo Imageable Dielectric. Since neither of these stack-ups have previously been electrically characterized, this paper characterizes both stack-ups up to 110 GHz using microstrip ring resonators (MRRs) and conductor backed coplanar waveguides (CBCPWs). Based on the characterization results, these stack-ups compare favorably against other stack-ups used for applications in this frequency range. After completing the electrical characterization, the Taiyo PID stack-up is also mechanically characterized for its flexibility using Free Arc Bending. The Free Arc Bending test shows that the ultra-thin glass stack-up is suitable for high frequency bending applications as the tested samples are capable of bending up to a separation of 33% of the sample's total length, displaying the capabilities of this ultra-thin glass substrate as a good candidate for a flexible substrate.**

Keywords—Glass, Microstrip Ring Resonators, Coplanar Waveguides, Free Arc Bending, Dielectric Constant, Dielectric Loss

I. Introduction

Due to the increasing consumer demand in wearable and flexible devices, developments in flexible technology have been occurring rapidly. Flexible technology focuses on maximizing mechanical flexibility while maintaining or improving electrical performance and system integration. Some areas of focus for flexible technology include RF and mmWave applications such as 5G communication and automotive radar. The characterization of various components for their individual responses are critical for designers to create these new systems, further helping the rapid development in flexible technology [1].

Flexible components should not experience any electrical performance differences or degradation compared to their rigid counterparts. A common technique used for flexible components include structures such as a serpentine pattern to minimize change in electrical performance while the component is stretched [2]. However, the major drawback with this approach is the increased DC resistance associated with the extra length the serpentine structure creates, thereby degrading the performance anyway. Other approaches include using flexible substrates such as Kapton polyimide and polyethylene terephthalate (PET) and flexible conductors such as silver inks. However, both types of flexible materials (substrates and conductors) present larger losses at higher frequencies (such as large loss tangent, low conductivity, and large surface roughness [3]), thereby limiting their applicability in emerging technologies such as 5G communication. Therefore, using new materials that are less lossy is critical for high frequency applications where maintaining flexibility becomes a necessity.

Glass-based substrates, compared to polyimide and PET, can have lower loss tangent and have lower surface roughness, making them a viable candidate for high frequency applications. Additionally, for applications such as automotive radar, glass has the additional advantage of higher glass transition temperature and a lower coefficient of thermal expansion [4]. Glass is already seen in flexible applications such as displays and photovoltaic cells so long as the glass is sufficiently thin for the application [5], [6], but has not been demonstrated for high frequency applications.

Information about the electrical dielectric properties of glass-based substrates have been shown up to 170 GHz in [7]. The glass substrates characterized in these studies typically includes a thicker glass core (at least 100 µm thickness). This paper in contrast will focus on thinner glass stack-ups (30 µm core glass thickness with 15 µm dielectric build up layers on each side). Thin glass is chosen as the core material in this paper as it could be used as a candidate for flexible applications. Therefore, this paper focuses first on the electrical characterization of these thin glass stack-ups to ensure that they are suitable for RF and mmWave applications. Afterwards, one of the glass stack-ups is mechanically characterized using Free Arc Bending to determine its effectiveness for flexible applications. The structure of the paper is divided into 4 parts. First, the fabrication of the glass samples for the electrical and mechanical characterization will be discussed. Next, the electrical characterization will be completed followed by mechanical characterization. Finally, the conclusion describes the viability of the thin glass stack-up for flexible RF and mm-Wave applications. To the best of the author's knowledge, this

XXX-X-XXXX-XXXX-X/XX/$XX.00 ©20XX IEEE

is the first demonstration of ultra-thin flexible glass being used for high frequency applications.

II. Fabrication of Flexible Glass Samples

The cross section of the test vehicles for the ultra-thin glass samples for electrical and mechanical characterization is shown in Fig. 1a and Fig. 1b respectively. Here, the core glass used is Schott AF32 30 µm thin glass [8] and its electrical properties can be seen in Table 1. This glass was chosen due to its favorable electrical characteristics while maintaining flexibility. Two separate buildup dielectrics were used for the electrical characterization, namely JSR GT-N01 [9] and Taiyo Photo Imageable Dielectric (PID) [10]. The electrical properties of these dielectrics can also be seen in Table 1. These buildup dielectrics were chosen due to their electrical performance and their overall thickness. The JSR GT-N01 was deposited on the glass using spin coating whereas the Taiyo PID film was vacuum laminated on the glass in 5 µm increments. Once the buildup dielectric was deposited onto the glass, the metallization for the electrical test vehicle was completed using the standard semi-additive process (SAP) where a TiCu (Ti thickness of 50 nm and Cu thickness of 400 nm) seed layer was deposited on each side of the glass substrate using physical vapor deposition. Afterwards, a negative tone photoresist (Hitachi RY5107) was used for photolithography using a mask aligner system. After photolithography, 6 µm of Cu was electroplated onto the sample followed by resist stripping and differential etching of the seed layer. The fabricated electrical characterization test vehicle can be seen in Fig. 2. For the mechanical test vehicle, the main difference between it and the electrical characterization test vehicle is the metallization method used. Instead of using the standard SAP process, screen printing was used instead. Here, Taiyo silver paste [11] is screen printed on to the Taiyo PID stack-up using a 50 µm thick, 325 stainless steel screen mesh. The thickness of the Ag paste after printing was found to be approximately 50 µm. The final fabricated mechanical flexibility characterization test vehicle can be seen in Fig. 3.

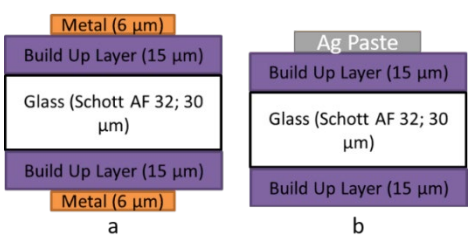

Fig. 1. The cross section of the test vehicle for (a) electrical and (b) mechanical characterization.

TABLE I. Electrical Properties of Materials used in The Ultra-Thin Glass Stack-ups

Material	Frequency (GHz)	ϵ_r	$\tan(\delta)$
Schott AF32	10	5.1	0.0061
	77	5.1	0.0114
	110	5.1	0.0128
JSR GT-N01 [9]	10	2.8	0.005
Taiyo PID [10]	10	3.3	0.019

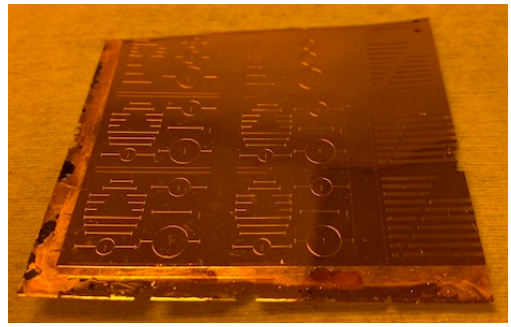

Fig. 2. Fabricated Electrical Characterization Test Vehicle

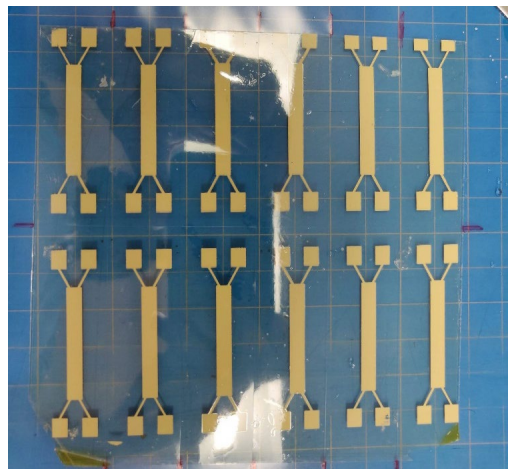

Fig. 3. Fabricated Mechanical Flexibility Characterization Test Vehicle.

III. Electrical Characterization

Both microstrip transmission lines and coplanar waveguides (CPWs) are common planar transmission lines used in RF and mmWave applications. As a result, these structures are used as the basis for the characterization in the form of microstrip ring resonators (MRRs) and via-less conductor backed CPWs (CBCPWs). For both the MRRs and the CBCPWs, the designed reference impedance was approximately 70Ω. This impedance was chosen as a means of ensuring compatibility with the measurement equipment as well as minimizing dispersion in the microstrip transmission lines.

A. Design of Microstrip Ring Resonator (MRR)

The MRR method for high frequency characterization of dielectric materials is both reliable and commonly used [7]. In this method, the relative dielectric constant (ϵ_r) at a given frequency is determined by the location of the resonant peaks. The relative dielectric constant at this frequency can be determined using (1).

$$f_n = \frac{nc}{2\pi r\sqrt{e_r}} \tag{1}$$

In (1), f_n corresponds to the nth resonant peak, c corresponds to the speed of light in free space, and r corresponds to the mean radius of the ring resonator. For this characterization, three separate rings were designed with fundamental frequencies of 10 GHz, 15 GHz, and 20 GHz. Additionally, TRL structures

were also included in the fabricated test vehicle to shift the reference plane to the end of the feed lines. The MRR structure can be seen in Fig. 4 with the designed radius for 10, 15, and 20 GHz.

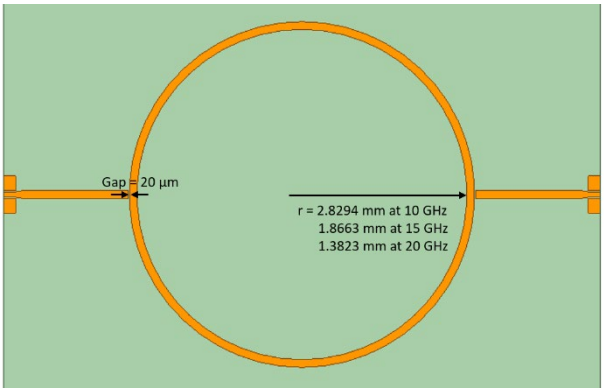

Fig. 4. The major MRR dimensions including the radius for 10, 15, and 20 GHz rings.

B. *Design of Conductor Backed Coplanar Waveguide (CBCPW) Lines*

The CPW lines were designed to be used to cross-correlate the results extracted from the microstrip ring resonator using ANSYS HFSS v19.1 [12]. The dimensions chosen for the CBCPWs match the measurement probe dimensions. To achieve an impedance close to 70Ω, a CBCPW (without vias) was used. The dimensions for this structure are shown in Fig. 5. These dimensions also match the dimensions of the probes used to measure the structures.

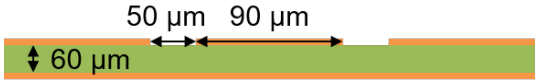

Fig. 5. CBCPW dimensions used to correlate the results for the MRR.

C. *Measurement Setup*

The measurement setup used is the same as the measurement setup in [7]. In this setup, an Anritsu ME7808 VNA with frequency extenders (3742A-EW) was used to measure the S Parameters up to 110 GHz. The probes used were the Cascade Micro Tech ACP-110-GSG-200 probes. The measurement setup was calibrated using LRRM calibration through the WinCal software. This was completed to remove any losses from the cables, test head, and probes and resulted in a variance of less than 0.1 dB in the thru standard throughout the entire frequency range.

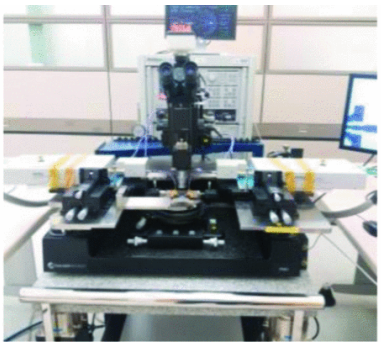

Fig. 6. The W Band measurement setup for electrical characterization measurements [7].

D. *MRR Measurement Results*

Multiple samples of the ring resonators for both the JSR and Taiyo stack-ups were fabricated and measured to minimize the error due to fabrication and measurement discrepancies. The measurements were completed using TRL de-embedding to remove the impact of the CPW probe pads, transitions, and feed lines. Example responses from the 15 GHz rings on the JSR and Taiyo stack-ups can be seen in Fig. 7a and Fig. 7b respectively.

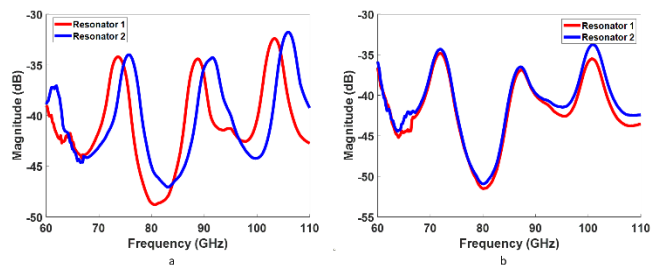

Fig. 7. The extracted Insertion Loss for both the JSR (a) and Taiyo (b) 15 GHz MRRs.

The relative dielectric constant for both the JSR and Taiyo stack-ups were extracted using the dispersive model described in [13]. The advantage of this model compared to the Quasi-Static model described in [14] is that this model includes dispersion effects, making it more accurate at higher frequencies. The results of this extraction are shown in Fig. 8a for both the JSR (squares) and Taiyo (triangles) stack-ups. For the JSR stack-up, the relative dielectric constant of 3.34±0.04 for the entire measured band and for the Taiyo stack-up, the dielectric constant is 3.68±0.07 for the entire band.

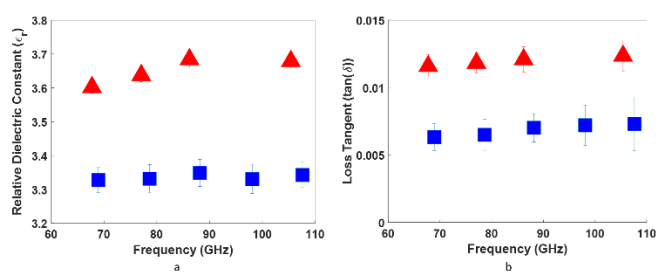

Fig. 8. The calculated relative dielectric constant (a) and the dielectric loss tangent (b) for the JSR (squares) and Taiyo (triangles) stack-up.

Extracting the dielectric loss tangent required the use of an indirect method. This method consisted of using the unloaded quality factor of the ring resonator as it includes both the conductor and dielectric losses. In this paper, the conductor losses were calculated and subtracted from the total loss to estimate the dielectric loss. Radiation losses are not considered as the ratio of line width to mean radius is significantly below 0.2 [14]. The calculated dielectric loss tangents are shown in Fig. 8b. For the JSR (squares) stack-up the dielectric loss tangent is between 0.0065 and 0.0075 and for the Taiyo (triangles) stack-up, the dielectric loss tangent is between 0.012 and 0.013, over the measured frequency range (60-110 GHz).

E. CBCPW Measurement Results

As discussed in Sec. III C, the CBCPWs were measured after completing the LRRM calibration. The measurement results for the JSR stack-up is shown in Fig. 9 and in Fig. 10 for the Taiyo stack-up. The length of the transmission line for the JSR sample in Fig. 9 was 8 mm while the length for the Taiyo sample in Fig. 10 was 7 mm. Additionally, these results were compared against simulated results for the CBCPWs based on the dielectric properties extracted from Sec. III D. These simulations were completed to act as a second comparison point between the extracted dielectric constant and dielectric loss tangent from the MRR data. These comparison simulations were completed using ANSYS HFSS v19.1 [12]. For both the JSR and Taiyo stack-ups, good correlation between the measured and simulated CBCPW S Parameters was found. This correlation further shows that the measured and extracted values found in the MRR measurement results are accurate. Additionally, Fig. 11 shows the per unit length loss for both stack-ups. The per unit length loss is 0.2 dB/mm and 0.3 dB/mm at 110 GHz for the JSR and Taiyo stack-ups respectively, indicating that both stack-ups should be useful for high frequency applications up to 110 GHz. A comparison between these stack-ups and other stack-ups used for W Band applications (70-110 GHz) is shown in Fig. 12.

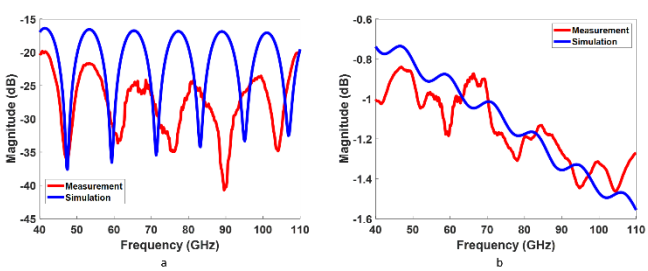

Fig. 9. The JSR stack-up CBCPW S11 (a) and S21 (b) response for a line length of 7 mm. The red curve corresponds to the measured result and the blue curve is the simulated result.

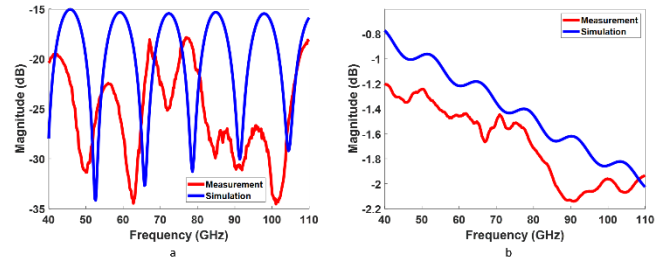

Fig. 10. The Taiyo stack-up CBCPW S11 (a) and S21 (b) response for a line length of 7 mm. The red curve corresponds to the measured result and the blue curve is the simulated result.

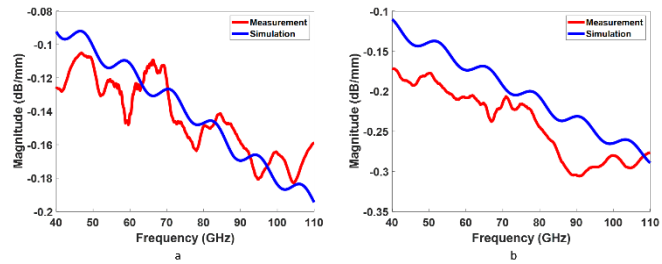

Fig. 11. The per unit length loss for the JSR stack-up (a) and the Taiyo stack-up (b). The red curve corresponds to the measured result and the blue curve is the simulated result.

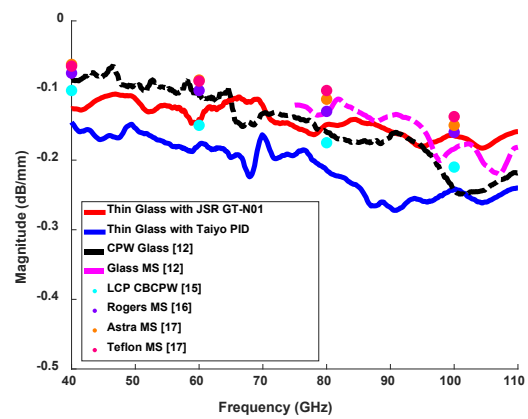

Fig. 12. Comparison between the materials used in this paper (solid lines) and other materials used for high frequency applications.

IV. Mechanical Flexibility

A. Mechanical Flexibility Test Setup

To determine the mechanical flexibility of the ultra-thin glass, Free Arc Bending was used, as shown in Fig. 13. In this test setup, the sample is inserted in the gap between two parallel plates with neither end fixed to the parallel plate, as shown in Fig. 13a. The ends of the sample are not fixed allowing the samples to be free to rotate. To ensure that the samples will not move along the length of the plate, a step, as indicated in Fig. 13c, is attached to each plate. These steps remain in contact with the sample to allow the sample to freely rotate while ensuring that the sample will remain attached to the plate, enabling the bending test to occur. The sample is not completely fixed to the parallel plates due to the brittleness of the glass as the stress

concentration on the fixture may break the glass before testing can even begin. In the test, as the top plate moves down (Fig. 13a to Fig. 13b and Fig. 13c), the sample is squeezed such that the bending radius of curvature decreases, creating stress and strain fields throughout the sample. The maximum stress and maximum strain on the sample occurs at the middle of the sample.

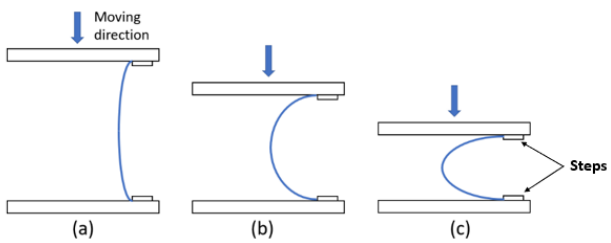

Fig. 13. The measurement setup to complete Free Arc Bending where (a) shows the initial measurement setup before bending, (b) shows the sample during the initial bending with a large radius of curvature, and (c) shows bending at the smallest radius of curvature.

For the Free Arc Bending tests, 4-point resistors were fabricated onto the bare Taiyo stack-up. The purpose of these 4-point resistors is to determine the distance between the two parallel plates when the sample fails (breaks). This distance then determines the minimum radius of curvature that the sample can experience before breaking. Additionally, these resistors will also show the impact of bending on the electrical performance of these resistors. If the change in resistance is substantial, new designs will need to be created to mitigate this impact. The size of glass stack-up used for each test sample in this test is 25 mm x 76 mm (1”x3”). For each test sample, a resistor of 38 mm (1.5”) length and 5 mm (0.2”) width is fabricated with 5 mm x 6.35 mm (0.2”x0.25”) probe pads. To measure the resistance of each resistor, a Keithley DMM6500 digital multimer (DMM) was connected to the resistor through Cu tape as shown in Fig. 14 and Fig. 15. In Fig. 14, the sample has each of the probe points connected to Cu tape and in Fig. 15, each side of the resistor is connected to pressure pads which then connects to the DMM. The final test setup for a single resistor sample can be seen in Fig. 16.

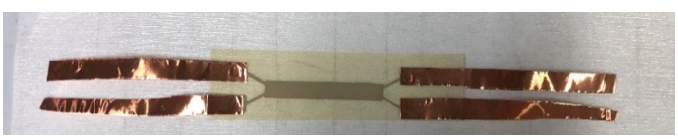

Fig. 14. Resistor sample with Cu tape to connect to the DMM.

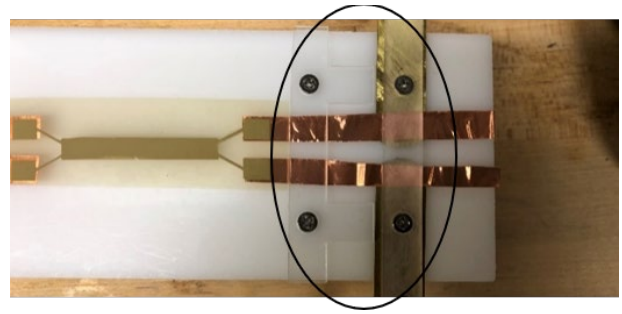

Fig. 15. Resistor sample connected on one side to the pressure contacts used for resistance measurement. The circled area includes the steps to connect the sample to a moving parallel plate in Fig. 16.

Fig. 16. Resistor sample inside of Free Arc Bending test setup.

B. Resistor Measurement Results

The resistors underwent 4 different types of mechanical tests, monotonic compressive (conductor facing inward) bending, monotonic tensile (conductor facing outward) bending, cyclical compressive bending, and cyclical tensile bending. The monotonic tests were completed to determine if and when the resistors would break while undergoing bending. The cyclical tests were completed to determine if the resistor samples could handle being bent and unbent in a repeated manner. In addition, the cyclical test shows the robustness of the ultra-thin glass stack-up while flexing. Both the compressive and tensile tests were completed to determine if the orientation of the sample would impact the bending capabilities of the glass stack-up. For the monotonic tests, a loading speed of 10 mm/min was used and for the cyclical tests, a loading speed of 60 mm/min was used. The results of the monotonic tests can be seen in Fig. 17 (compressive bending) and Fig. 18 (tensile bending) and the results of the cyclical tests can be seen in Fig. 19 (compressive bending) and Fig. 20 (tensile bending). For both the compressive and tensile monotonic tests, the resistance (0.27 Ω and 0.22 Ω respectively) remained stable until the sample broke. The breaking point for both the compressive and tensile bending samples was past 50 mm of distance travelled, which corresponds to a radius of curvature below 12.5 mm radius, or 0.5”, which is below 17% of the total length of the sample. For

compressive bending, the sample broke at 51 mm distance travelled and the tensile bending sample broke at 60 mm distance travelled. Therefore, for the cyclical tests, the samples were set to travel 50 mm before returning to the starting position. In both the compressive and tensile cyclical tests, the samples completed at least nine cycles of bending. The compressive bending sample broke at the bottom portion (maximum bending) of the final cycle, indicative of the accumulation of stresses along the sample. This is to be expected as the compressive monotonic test showed the sample break around this point. Additionally, the cyclical test undergoes increased load due to the increased loading speed on the samples. Since the monotonic tensile test had the resistor break at approximately 60 mm distance travelled, it is to be expected that the sample would last the full cyclical tensile test. For both the compressive and tensile cyclical tests, similar to the monotonic versions, the resistance remained stable, indicating that bending does not have a significant impact on the resistance. A summary of the monotonic and cyclical bending results can be seen in Tables 1 and 2 respectively. One future improvement for this work will be to include more samples in the bending tests to determine the statistical distribution of the failure of the glass stack-up to acquire the full mechanical properties of the stack-up. These mechanical properties are a function of the pre-damage on the samples, which will be altered by the damage on the corners and edges of the samples will dicing the larger substrate into smaller samples.

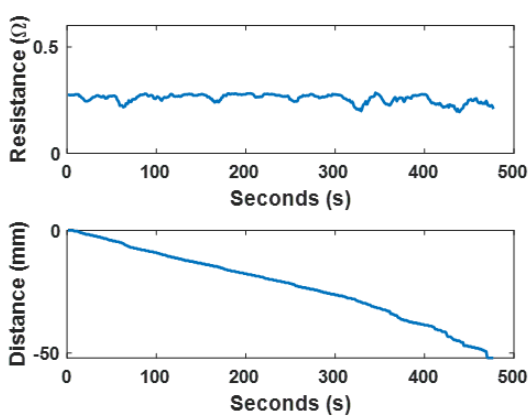

Fig. 17. Change in resistance for the resistor undergoing monotonic compressive bending. The distance refers to the distance travelled by the moving jig.

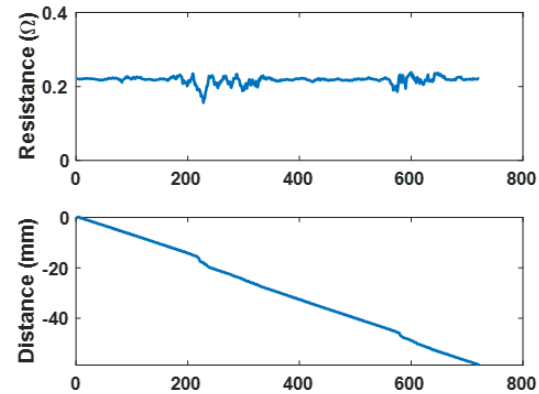

Fig. 18. Change in resistance for the resistor undergoing monotonic tensile bending. The distance refers to the distance travelled by the moving jig.

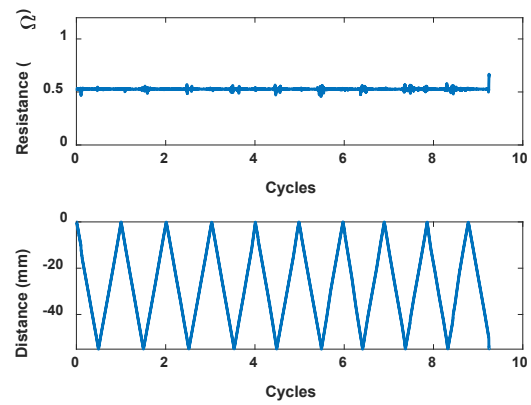

Fig. 19. Change in resistance for the resistor undergoing cyclical compressive bending. The distance refers to the distance travelled by the moving jig.

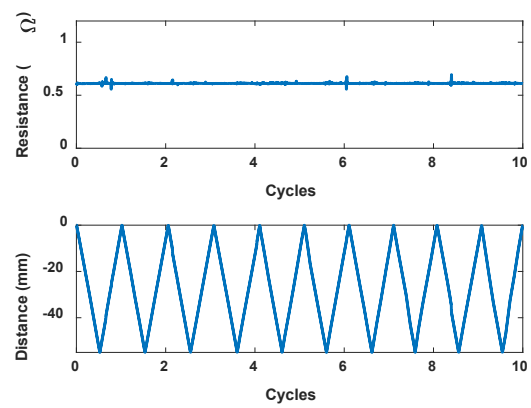

Fig. 20. Change in resistance for the resistor undergoing cyclical tensile bending. The distance refers to the distance travelled by the moving jig.

TABLE II. MONOTONIC BENDING RESULTS

Type of Bending	Loading Rate	Failure Point (distance travelled to break sample)	Minimum Radius of Curvature	Resistance
Compressive Bending	10 mm/min	51 mm	12.5 mm	0.27 Ω
Tensile Bending	10 mm/min	60 mm	8 mm	0.22 Ω

TABLE III. CYCLICAL BENDING RESULTS

Type of Bending	Loading Rate	Maximum Distance Travelled	Minimum Radius of Curvature	Total Cycles Completed	Resistance
Compressive Bending	60 mm/min	50 mm	13 mm	9	0.52 Ω
Tensile Bending	60 mm/min	50 mm	13 mm	10	0.60 Ω

V. CONCLUSION

In this paper, we show the initial results on the performance of flexible, ultra-thin glass for RF applications. Based on the electrical characterization of the two separate glass stack-ups discussed, the stack-up is suitable for applications up to 110 GHz. For the JSR stack-up, the measured loss at 110 GHz was measured to be 0.2 dB/mm ±6% and for the Taiyo stack-up, the per unit length loss was 0.3 dB/mm ±3%. Based on these per unit length results, both stack-ups compare favorably against other stack-ups used for applications in high frequency applications. Additionally, as shown with the Taiyo stack-up, the glass stack-up is suitable for flexible applications until the sample is bent to a separation of 33% of its original length, which corresponds to a radius of curvature 17% of the original length of the sample. Based on these results, the glass could be suitable for both applications where the glass substrate stays in a conformal state (a state of remaining bent) or in a cyclical state. Overall, this investigation concludes that this flexible, ultra-thin glass substrate material is suitable for flexible applications up to 110 GHz, the first of its kind.

ACKNOWLEDGMENT

This work was supported by the Industry Consortium at the Georgia Tech Packaging Research Center (PRC). The authors would like to thank JSR, Schott, and Taiyo for supplying materials for this research. The authors would also like to thank Lila Dahal and Mohanalingam Kathaperumal in supporting the fabrication experiments.

REFERENCES

[1] L. Shao, T. C. Huang, T. Lei, Z. Bao, R. Beausoleil and K. T. Cheng, "Process design kit for flexible hybrid electronics," 2018 23rd Asia and South Pacific Design Automation Conference (ASP-DAC), Jeju, Korea (South), 2018, pp. 651-657.

[2] J. W. Jeon et al., "Electrical characterization of differential stretchable transmission line," 2011 IEEE MTT-S International Microwave Symposium, Baltimore, MD, 2011, pp. 1-4.

[3] S. Swaisaenyakorn, P. R. Young and M. Shkunov, "Characterization of ink-jet printed CPW on Kapton substrates at 60 GHz," 2014 Loughborough Antennas and Propagation Conference (LAPC), Loughborough, 2014, pp. 676-678.

[4] S. M. Garner, S. C. Lewis and D. Q. Chowdhury, "Flexible glass and its application for electronic devices," 2017 24th International Workshop on Active-Matrix Flatpanel Displays and Devices (AM-FPD), Kyoto, 2017, pp. 28-33.

[5] S. M. Garner et al., "Cholesteric Liquid Crystal Display With Flexible Glass Substrates," in Journal of Display Technology, vol. 9, no. 8, pp. 644-650, Aug. 2013.

[6] F. Ballipinar, A. C. Rastogi, S. M. Garner and S. B. Darling, "Planar mixed halide perovskite-PCBM solar cells on flexible glass substrates processed at low temperature without ITO," 2016 IEEE 43rd Photovoltaic Specialists Conference (PVSC), Portland, OR, 2016.

[7] M. u. Rehman, S. Ravichandran, S. Erdogan and M. Swaminathan, "W-band and D-band Transmission Lines on Glass Based Substrates for Sub-THz Modules," *2020 IEEE 70th Electronic Components and Technology Conference (ECTC)*, Orlando, FL, USA, 2020, pp. 660-665

[8] Electrical Properties of SCHOTT Thin Glasses Datasheet

[9] H. Ito *et al*., "Advanced Low-Loss and High-Density Photosensitive Dielectric Material for RF/Millimeter-Wave Applications," *2019 International Wafer Level Packaging Conference (IWLPC)*, San Jose, CA, USA, 2019, pp. 1-6

[10] D. Okamoto *et al*., "Fabrication and Reliability Demonstration of 3 µm Diameter Photo Vias at 15 µm Pitch in Thin Photosensitive Dielectric Dry Film for 2.5 D Glass Interposer Applications," *2019 IEEE 69th Electronic Components and Technology Conference (ECTC)*, Las Vegas, NV, USA, 2019, pp. 2112-2116

[11] Taiyo's silver paste product Datasheet

[12] Ansys 19.1, Jan. 2021, [online] Available: http://www.ansys.com

[13] I. Wolff and N. Knoppik, "Microstrip ring resonator and dispersion measurement on microstrip lines", *Electronics Letters*, vol. 7, no. 26, pp. 779-781, December 1971.

[14] M. Kirschning and R.H. Jansen, "Accurate Model for Effective Dielectric Constant of Microstrip with Validity up to mm-wave Frequencies", *Electonics Letters*, vol. 18, no. 6, pp. 272-273, 1982.

[15] D. Thompson, P. Kirby, J. Papapolymeron and M. M. Tentzeris, "W-band characterization of finite ground coplanar transmission lines on liquid crystal polymer (LCP) substrates," *53rd Electronic Components and Technology Conference, 2003. Proceedings.*, New Orleans, Louisiana, USA, 2003, pp. 1652-1655

[16] F. Fesharaki, T. Djerafi, M. Chaker and K. Wu, "Guided-Wave Properties of Mode-Selective Transmission Line," in *IEEE Access*, vol. 6, pp. 5379-5392, 2018

[17] Astra MT77, A Teflon Replacement, Isola, 2017.